

Sulfated graphene as an efficient solid catalyst for acid-catalyzed liquid reactions

Fujian Liu,^b Jing Sun,^c Longfeng Zhu,^c Xiangju Meng,^a Chenze Qi^b and Feng-Shou Xiao^{*a}

Received 15th December 2011, Accepted 25th January 2012

DOI: 10.1039/c2jm16608a

Graphene with its two-dimensional sheet of sp²-hybridized carbon is a hot topic in the fields of materials and chemistry due to its unique features. Herein, we demonstrate that sulfated graphene is an efficient solid catalyst for acid-catalyzed liquid reactions. The sulfated graphene was synthesized from a facile hydrothermal sulfonation of reduced graphene oxide with fuming sulfuric acid at 180 °C. Combined characterizations of XRD, Raman, and AFM techniques show that G-SO₃H has a sheet structure (1–4 layers). IR spectroscopy shows that G-SO₃H has a S=O bond, and the XPS technique confirms the presence of an S element in G-SO₃H. Acid–base titration indicates that the acidic concentration of sulfonic groups in the sulfated graphene is 1.2 mmol g⁻¹. TG curves shows that the decomposition temperature (268 °C) of the sulfonic groups on the sulfated graphene is much higher than that of conventional SO₃H-functionalized ordered mesoporous carbon (237 °C). Catalytic tests of the esterification of acetic acid with cyclohexanol, the esterification of acetic acid with 1-butanol, the Peckmann reaction of resorcinol with ethyl acetoacetate, and the hydration of propylene oxide show that sulfated graphene is much more active than the conventional solid acid catalysts of Amberlyst 15, OMC-SO₃H, SO₃H-functionalized ordered mesoporous silica (SBA-15-SO₃H), graphene oxide, and reduced graphene oxide, which is attributed to the fact that the sulfated graphene almost has no limitation of mass transfer due to its unique sheet structure. Very importantly, the sulfated graphene has extraordinary recyclability in these reactions, which is attributed to the stable sulfonic groups on the sulfated graphene. The advantages, including high activities and good recyclability as well as simple preparation, are potentially important for industrial applications of the sulfated graphene as an efficient heterogeneous solid acid catalyst in the future.

Introduction

The replacement of mineral liquid acids by solid acids for the production of fine chemicals by acid-catalyzed liquid reactions has attracted much attention, due to the obvious advantages of heterogeneous catalysts, including easy separation of the catalyst from the reaction medium, reductive corrosion, and improved regenerability.^{1–5} Typically, solid acids are porous materials such as zeolites,^{1–5} mesoporous materials,^{6–8} ion-exchange resins,⁹ and SO₃H-functionalized porous carbons.^{10,11} Among these porous solid acids, catalytically active acidic sites are mainly located in the pores of the catalysts, therefore the mass transfer to and from the active sites in the pores plays an important role for catalytic performance,^{1–11} in particular for acid-catalyzed liquid reactions.^{12–15}

To reduce the limitation of mass transfer in catalysis, various strategies, such as the synthesis of nanosized zeolites and the preparation of hierarchical porous materials, have been successfully pursued.^{16–23} They exhibit much better catalytic properties than conventional porous catalysts due to a significant increase in mass transfer in the reactions.^{12–23} More recently, Ryoo *et al.* have fabricated single-unit-cell nanosheets of zeolites with extraordinary mass transfer from the unique bifunctional surfactant templates,^{24,25} but their catalytic applications are influenced by the use of relatively high-cost templates.

It is well known that graphene, a two-dimensional sheet of sp²-hybridized carbon discovered by Geim and co-workers in 2004,^{26–28} has been widely used in the fields of nanoelectronic devices,^{29–31} sensors,^{32,33} catalysis,^{34–41} adsorption,⁴² and energy storage^{43–46} due to its excellent thermal and mechanical stabilities, superior electrical conductivity, very high degree of exposure of active sites on the surface, and its outstanding dispersion in various systems.^{26–28,47–50} In spite of many successful examples of using graphene as a catalyst support in recent years,^{34–41} to the best of our knowledge, there is still no report of using sulfated graphene as an efficient solid acid catalyst.

^aDepartment of Chemistry, Zhejiang University, Hangzhou 310028, China. E-mail: fshxiao@zju.edu.cn; Fax: +86-431-85168590; Tel: +86-431-85168590

^bInstitute of Applied Chemistry, Shaoxing University, Shaoxing, 312000, China

^cDepartment of Chemistry, Jilin University, Changchun 130012, China

Herein, we demonstrate a facile synthesis of sulfated graphene (G-SO₃H) from hydrothermal sulfonation by fuming sulfuric acid at a relatively high temperature (180 °C). Very importantly, G-SO₃H exhibits much better catalytic properties (activity and recyclability) than conventional porous solid acids such as SO₃H-functionalized ordered mesoporous carbon (OMC-SO₃H), Amberlyst 15, and SO₃H-functionalized ordered mesoporous silica (SBA-15-SO₃H) in acid-catalyzed liquid reactions including the esterification of acetic acid with cyclohexanol, the esterification of acetic acid with 1-butanol, the Peckmann reaction of resorcinol with ethyl acetoacetate, and the hydration of propylene oxide.

Experimental

Synthesis

Chemicals and reagents. Amberlyst 15 and the nonionic block copolymer surfactant poly(ethyleneoxide)-poly(propyleneoxide)-poly(ethyleneoxide) block copolymer (Pluronic 123, molecular weight of about 5800) were purchased from Sigma-Aldrich Company. Graphite, sodium nitrate (NaNO₃), potassium permanganate (KMnO₄), sodium borohydride (NaBH₄), sulfuric acid (H₂SO₄), cyclohexanol, acetic acid, resorcinol, ethyl acetoacetate, toluene, propylene oxide, 1-butanol, phenol, formaldehyde (37 wt%), tetraethyl orthosilicate (TEOS), fuming sulfuric acid, and 3-mercaptopropyltrimethoxysilane (3-MPTS), were obtained from Tianjin Guangfu Chemical Reagent Co.

Synthesis of graphene oxide (GO) and reduced graphene oxide (RGO). The GO dispersion was prepared using Hummers-method as described previously.⁵¹ As a typical run, (1) 5.0 g of graphite power was added into a mixture of 5.0 g of NaNO₃ and 120 mL of H₂SO₄ (98%) in a 500 mL flask. (2) After stirring for 30 min in an ice bath, 30 g of KMnO₄ was slowly added under vigorous stirring. (3) After stirring at room temperature over 12 h, the mixture gradually became paste-like and the color turned light brownish. (4) After the addition of 300 mL water under stirring, the mixture was heated to 98 °C in a short time and kept at this temperature for 24 h, giving a yellow sample. (5) 100 mL of H₂O₂ (50 wt%) was added to the mixture, stirring for 24 h at room temperature. (6) After rinsing and centrifugation with 5% HCl and deionized water several times, the GO dispersion was obtained.

RGO was synthesized by the chemical reduction of GO using sodium borohydride. As a typical run, 0.5 g of the GO dispersion was added into water (500 mL), followed by sonication for 30 min. Then, 1.2 g of sodium borohydride was added into the mixture, heating at 100 °C for 24 h. After repeated washing with water and centrifugation, and dispersing in the water, RGO was finally obtained.

Hydrothermal sulfonation of graphene (G-SO₃H). G-SO₃H was synthesized from the hydrothermal sulfonation of RGO using fuming sulfuric acid at 180 °C. As a typical run, 1.0 g of RGO was added into 50 mL of fuming sulfuric acid. After sonication for 30 min, the mixture was transferred into an autoclave to heat at 180 °C for 24 h under stirring. After washing with a large amount of water and drying at 80 °C for 12 h under vacuum, G-SO₃H was finally obtained.

In comparison, SBA-15-SO₃H and OMC-SO₃H were synthesized as in the literature.^{6,52}

Characterization

X-Ray diffraction (XRD) patterns were recorded on a Rigaku D/Max-2550 using nickel-filtered Cu K α radiation. FTIR spectra were recorded by using a Bruker 66V FTIR spectrometer. XPS spectra were performed on a Thermo ESCALAB 250 with Al K α radiation, and binding energies were calibrated using the C1s peak at 284.9 eV. Thermogravimetric analysis (TG) was performed on a Perkin-Elmer TGA7 in flowing air with a heating rate of 10 °C min⁻¹. Atomic force micrographs (AFM) were obtained using a NanoWizard II BioAFM (JPK Instrument AG, Berlin, Germany) in tapping mode. Raman spectra were obtained with a Renishaw Raman system model 1000 spectrometer.

Catalytic reactions

Before reaction, the catalysts were activated by 0.1 M H₂SO₄ for 4 h at room temperature. Esterification of acetic acid with cyclohexanol (EAC), esterification of acetic acid with butanol (EAB), the Peckmann reaction of resorcinol with ethyl acetoacetate (PRE), and hydration of propylene oxide (HPO) were chosen as the models for acid-catalyzed liquid reactions.

EAC was performed by mixing 0.2 g of catalyst, 17.5 mL (305 mmol) of acetic acid, and 11.5 mL (110 mmol) of cyclohexanol in a three-necked round-bottomed flask equipped with a condenser and a magnetic stirrer. After heating the mixture to 100 °C in an oil bath under stirring, 17.5 mL (305 mmol) of acetic acid were rapidly added, and the reaction lasted for 5 h. In this reaction, the molar ratio of acetic acid to cyclohexanol was 2.8 and the mass ratio of catalyst to cyclohexanol was 0.018. The product was cyclohexyl acetate with a selectivity of nearly 100%.

EAB was performed by mixing 0.01 g catalyst, 50 mmol of acetic acid and 50 mmol of butanol in a glass flask equipped with a condenser and a magnetic stirrer. After heating the mixture to 90 °C, the reaction lasted for 4 h. In this reaction, the molar ratio of acetic acid to butanol was 1.5 and the mass ratio of catalyst to butanol was 0.0027. The product was *n*-butylacetate with a selectivity of nearly 100%.

PRE was performed by mixing 0.2 g of catalysts, 10 mmol of resorcinol, and 10 mmol of ethyl acetoacetate in a glass flask equipped with a condenser and a magnetic stirrer. After the addition of 10 mL toluene solvent, the temperature was increased to 110 °C in an oil bath under stirring. The reaction lasted for 2 h. In this reaction, the molar ratio of resorcinol to ethyl acetoacetate was 1.0 and the mass ratio of catalyst to ethyl acetoacetate was 0.15. The product was 7-hydroxy-4-methylcoumarin with a selectivity of nearly 100%.

HPO was performed by mixing 0.1 g of catalyst, 50 mmol of propylene oxide, and 500 mmol of H₂O in a glass flask equipped with a condenser and a magnetic stirrer. The reaction lasted for 6 h at 27 °C under stirring. The molar ratio of propylene oxide to water was 0.1 and the mass ratio of catalyst to water was 0.011. The product was 1,2-propylene glycol with a selectivity of nearly 100%.

The products in these reactions were analyzed by gas chromatography (Shimadzu 14C and Agilent 7890) with a flame ionization detector (FID), and dodecane was used as an internal standard. The column was OV-1 (30 m), the temperature region was 100–220 °C with a rate of 20 °C min⁻¹, and the temperature of the FID detector was 280 °C. In these reactions, the stirring rate was 800 rpm.

Results and discussion

Normally, the sulfonation of graphene is carried out with the aryl diazonium salts of sulfanilic acid.^{53,54} In this work, a sulfated graphene (G-SO₃H) is synthesized from the hydrothermal sulfonation of RGO by fuming sulfuric acid at 180 °C. Compared with a conventional route, the hydrothermal sulfonation is very simple and the use of aryl diazonium salts is completely avoided, which could be very useful for industrial applications.

Fig. 1 shows the XRD patterns of graphite, graphene oxide (GO), RGO, and G-SO₃H. Graphite gives a strong peak at 26.5° (Fig. 1a). However, GO only shows a peak at 12.6° and the peak at 26.5° associated with graphite completely disappears (Fig. 1b), indicating the successful insertion of oxygen species between the graphitic layers.⁵⁵ After the reduction of GO by sodium borohydride, RGO shows a disappearance of the diffraction peak at 12.6° associated with GO and the reappearance of the very weak and broad diffraction peak ranging from 21.3 to 27.6°, centered at 24.1° (Fig. 1c), suggesting that GO is reduced to graphene with only a few layers.⁵⁶ After hydrothermal sulfonation, G-SO₃H has a very similar XRD pattern to RGO (Fig. 1d), suggesting their similar graphene layers.

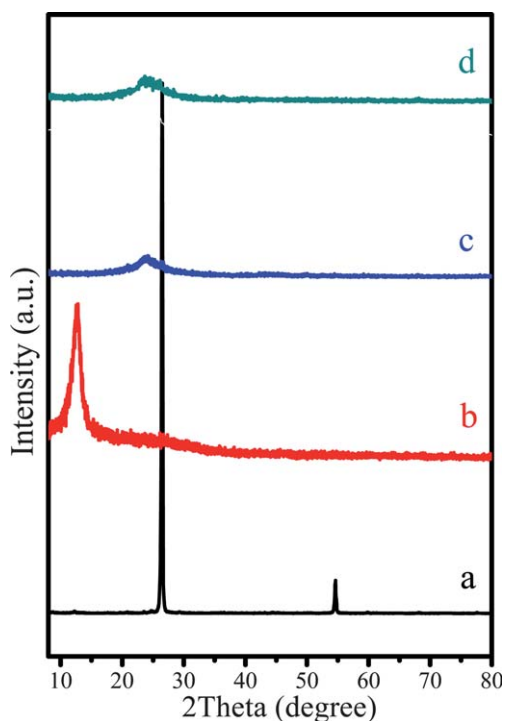


Fig. 1 XRD patterns of (a) graphite, (b) GO, (c) RGO, and (d) G-SO₃H.

Fig. 2 shows the Raman spectra of graphite, GO, RGO, and G-SO₃H. Graphite displays a prominent G peak at 1581 cm⁻¹, corresponding to the first-order scattering of the E_{2g} mode.⁵⁷ In contrast, GO shows peaks at 1594 and 1363 cm⁻¹, which are attributed to the G band (the vibration of sp² carbon atoms in a graphitic 2D hexagonal lattice) and the D band (the vibrations of sp³ carbon atoms of defects and disorder), respectively.^{58,59} RGO and G-SO₃H exhibit similar Raman spectra to GO, but their intensity ratios of D to G bands are a little different (Fig. 2c & 2d). Compared with GO (0.89), G-SO₃H gives a relatively high ratio of D : G (1.02), suggesting a decrease in the average size of the sp² carbon domains by the formation of sp³ carbons due to the incorporation of oxygen or sulfur heteroatoms during the chemical treatment.^{53,54}

Fig. 3 shows the FT-IR spectra of RGO and G-SO₃H. Compared with RGO, G-SO₃H exhibits an additional band at 1090 cm⁻¹, which is associated with a S=O bond,^{60,61} indicating the successful grafting of SO₃H groups onto graphene. It is worth noting that the peak at 1720 cm⁻¹ for both samples is assigned to a C=O bond, attributed to the lower content of unreduced oxygen atoms on the samples.^{60,61} Furthermore, we evaluated the number of acidic sites over G-SO₃H by using an acid–base titration, which gives 1.2 mmol g⁻¹. This value is comparable with that of OMC-SO₃H (1.3 mmol g⁻¹),⁵² but still much lower than that of Amberlyst 15 (4.7 mmol g⁻¹).

Fig. 4 shows the X-ray photoelectron spectrum (XPS) of G-SO₃H, which gives signals mainly associated with C1s, O1s, and S2p, confirming the presence of a sulfur element in G-SO₃H, in good agreement with the IR results. The high resolution C1s

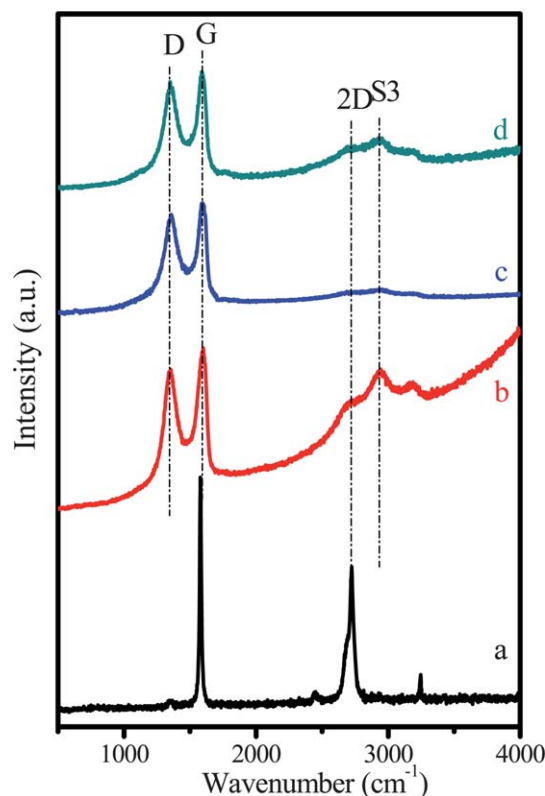


Fig. 2 Raman spectra of (a) graphite, (b) GO, (c) RGO, and (d) G-SO₃H.

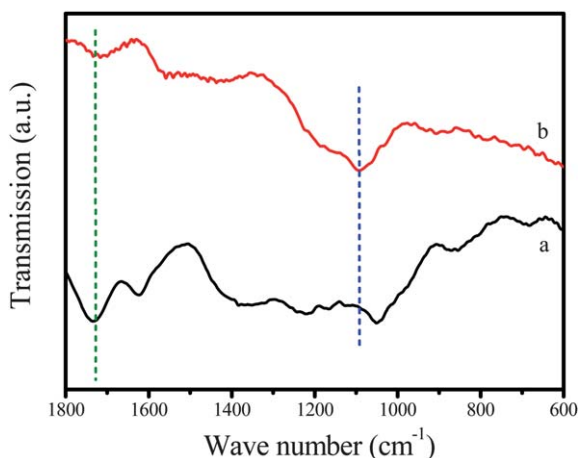


Fig. 3 FT-IR spectra of (a) R-GO and (b) G-SO₃H.

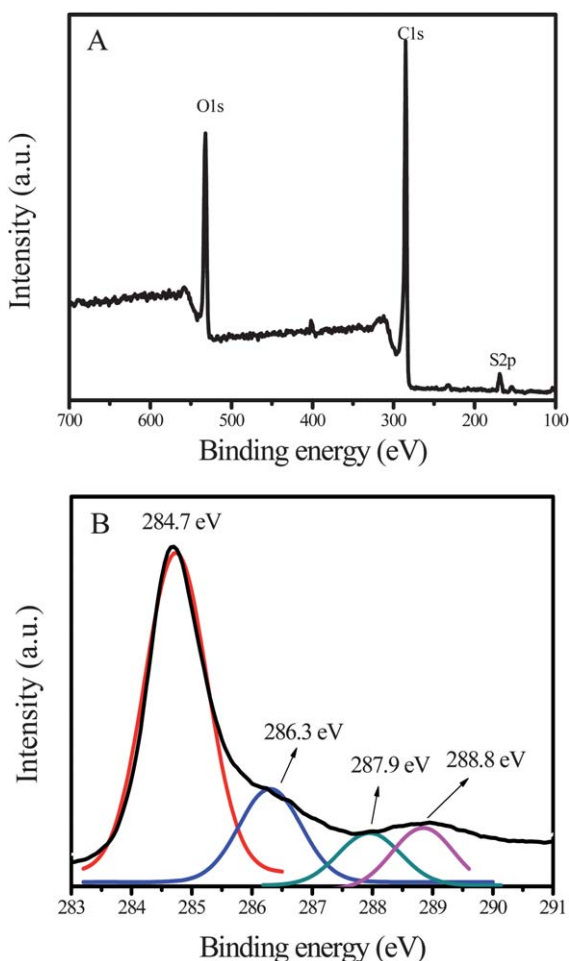


Fig. 4 (A) XPS spectrum and (B) high-resolution C1s spectrum of G-SO₃H.

XPS spectrum (Fig. 4b) shows peaks at 284.7, 286.3, 287.9, and 288.8 eV, which are attributed to the non-oxygenated ring carbon, the carbon in the C–O bond, the carbonyl carbon, and the carboxylated carbon, respectively. Obviously, the peak at 284.6 eV is dominant, suggesting that most of the

oxygen-containing functional groups have been successfully removed in G-SO₃H. Fig. 5 shows the S2p spectrum of G-SO₃H, OMC-SO₃H, and Amberlyst 15. G-SO₃H displays a peak at 168.3 eV associated with a S–O bond (Fig. 5a), which is slightly lower than those (168.8 and 168.9 eV) of G-SO₃H and OMC-SO₃H. The shift to low binding energy is explained by the electron transfer from graphene to the SO₃H group,^{26–28} which might result in a decrease in acidic strength for the SO₃H group in G-SO₃H.

Fig. 6 shows an atomic force microscopic (AFM) image of G-SO₃H, confirming the sheet morphology. The thickness of the sample is estimated at 0.8–3.0 nm, which corresponds to 1–4 graphene sheets, in good agreement with those reported previously.^{26–28,62} These results indicate that the sheet structure of graphene is well retained after the hydrothermal sulfonation.

Fig. 7 showed the TEM images of G-SO₃H and OMC-SO₃H. Clearly, the G-SO₃H sample appears transparent, which is similar to that of single graphene sheets,⁶² in good agreement with the AFM results. Additionally, the OMC-SO₃H sample exhibits a highly ordered mesostructure, as published in the literature.⁵²

Fig. 8 shows the TG curves of G-SO₃H and OMC-SO₃H. OMC-SO₃H exhibits two obvious weight losses centered at 237 and 390 °C, which are assigned to the decomposition of sulfonic groups and the sample framework. In contrast, G-SO₃H shows a much higher temperature for the decomposition of sulfonic groups and the sample framework, at 268 and 568 °C, respectively. These results indicate that G-SO₃H has much better thermal stability than OMC-SO₃H, which would be potentially important for recycling catalysts. The higher temperature for the decomposition of sulfonic groups over G-SO₃H than that over OMC-SO₃H is attributed to the stronger interaction of graphene with the sulfonic group, as evidenced by S2p spectroscopy (Fig. 5); The better stability of the framework on G-SO₃H than that on OMC-SO₃H is attributed to the fact that the carbon of OMC-SO₃H is amorphous while the carbon of G-SO₃H is graphene.

Table 1 presents the acidic contents and catalytic data for the esterification of acetic acid with cyclohexanol (EAC), the esterification of acetic acid with 1-butanol (EAB), the Peckmann

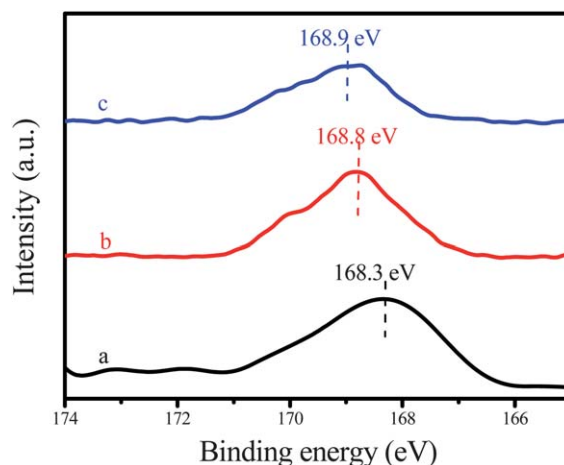


Fig. 5 S2p spectra (a) G-SO₃H, (b) OMC-SO₃H, and (c) Amberlyst 15.

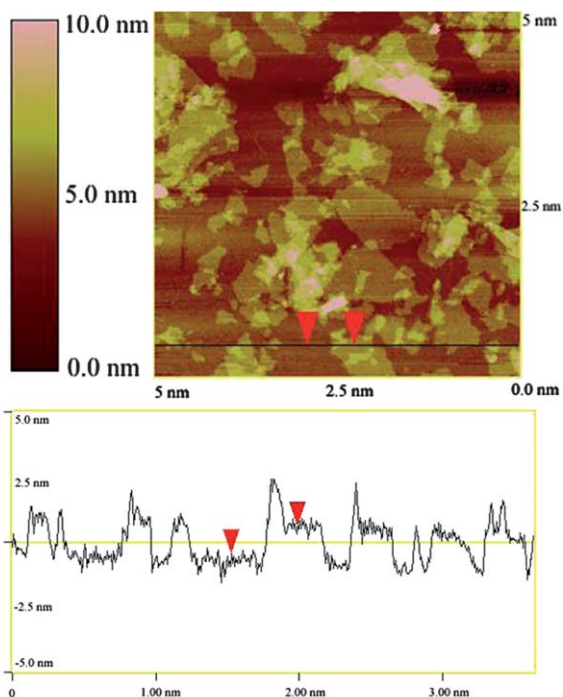


Fig. 6 (A) AFM image of G-SO₃H and (B) corresponding thickness analysis.

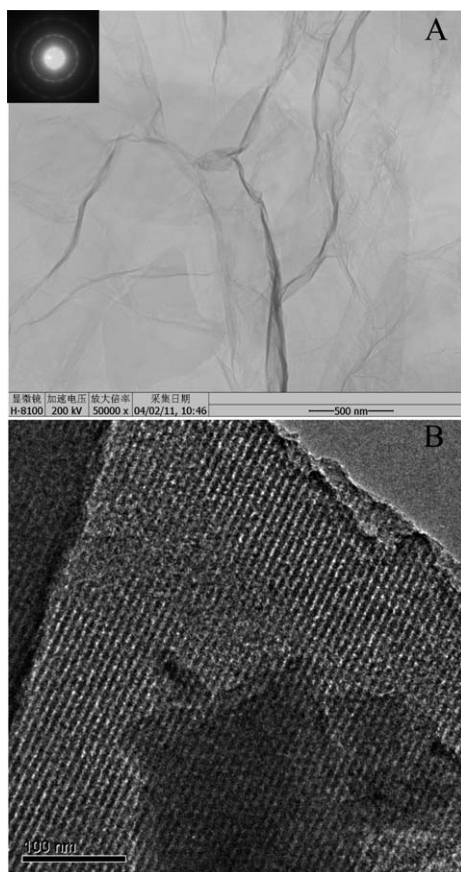


Fig. 7 TEM images of (A) G-SO₃H and (B) OMC-SO₃H.

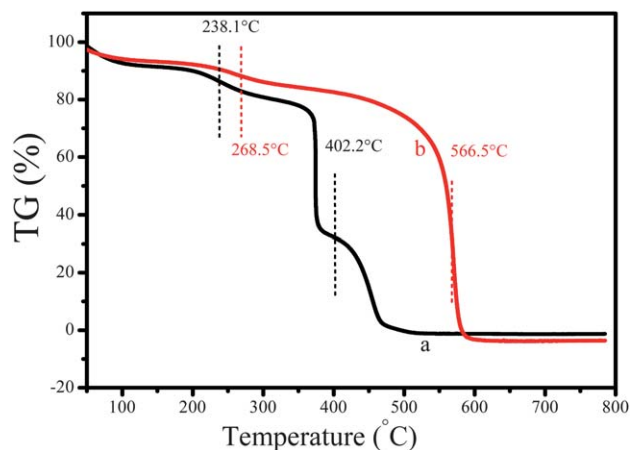
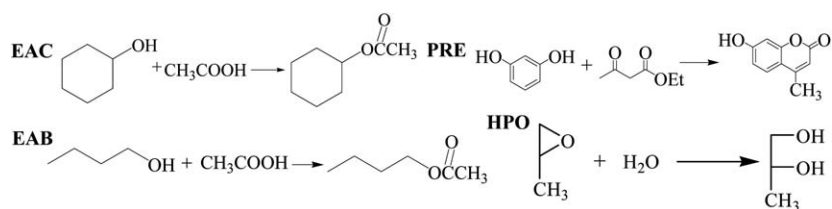


Fig. 8 TG curves of (a) OMC-SO₃H and (b) G-SO₃H.

reaction of resorcinol with ethyl acetoacetate (PRE), and the hydration of propylene oxide (HPO) over various catalysts. Clearly, it is observed that G-SO₃H (Table 1, run 1–3) shows much higher catalytic activities than those of OMC-SO₃H, SBA-15-SO₃H, Amberlyst 15, GO, and RGO (Table 1, run 4–10) in EAC. For example, G-SO₃H gives a conversion to cyclohexanol of 79.5% (Table 1, run 1), while OMC-SO₃H, Amberlyst 15, GO and RGO give conversions of 52.2, 58.9, 11.5 and 10.2% (Table 1, run 4, 7, 9, and 10), respectively. Interestingly, GO and RGO show very low activities, which is attributed to the absence of acidic sites on the samples, as confirmed by acid–base titration and S analysis. Considering the similar acidic content of G-SO₃H to OMC-SO₃H and the higher acidic content of Amberlyst 15 than G-SO₃H (Table 1) as well as the weaker acidic strength of G-SO₃H than OMC-SO₃H and Amberlyst 15 (Fig. 5), the higher catalytic activities over G-SO₃H than OMC-SO₃H and Amberlyst 15 should be directly assigned to the difference in the sample structure. G-SO₃H has a sheet structure, and almost all of the sulfonic groups are exposed to the reactants, where there is no limitation for mass transfer (Fig. 9a) due to the novel nanosheet structure. In addition, the novel nanosheet structure is also favorable for the high dispersion of sulfonic groups, and most of the sulfonic groups are accessible to reactants.⁶¹ On the contrary, OMC-SO₃H and Amberlyst 15 (Fig. 9b) are porous materials, and the reaction is strongly dependent on the mass transfer through the pores which exist in the samples. In addition, some of the sulfonic groups over these catalysts might not be accessible to reactants. To check this idea, catalytic activities over OMC-SO₃H and G-SO₃H under static conditions have been measured. The results show that there are almost the same activities over G-SO₃H at a stirring rate of 800 rpm (79.5%, Table 1, run 1) and at static conditions (78.9%, Table 1, run 2), in good agreement with those (94.3 and 94.8% under stirring and static conditions in EAC, respectively) of sulfuric acid (98%), a typical homogeneous acid catalyst. However, OMC-SO₃H has obvious differences in catalytic activities between the stirring (52.2%, Table 1, run 4) and static (42.1%, Table 1, run 5) conditions.

Fig. 10 shows the catalytic kinetic curves of G-SO₃H, OMC-SO₃H, and Amberlyst 15 in the EAC. Typically, G-SO₃H has a three-step profile. The first stage is the first 1 h and the reaction is performed at high rate; the second stage in the time range of

Table 1 Acidic contents and catalytic activities for esterification of acetic acid with cyclohexanol (EAC), esterification of acetic acid with 1-butanol (EAB), the Peckmann reaction of resorcinol with ethyl acetoacetate (PRE), and hydration of propylene oxide (HPO) over various catalysts



Run	Catalysts	Acid sites/mmol g^{-1} ^a	EAC conv. (%)	EAB conv. (%)	PRE conv. (%)	HPO yield. (%)
1	G-SO ₃ H	1.2	79.5	89.1	82.1	66.8
2	G-SO ₃ H ^b	1.2	78.9	89.3	81.7	66.4
3	G-SO ₃ H ^c	1.13	78.3	87.2	80.8	64.9
4	OMC-SO ₃ H	1.3	52.2	75.1	66.1	42.3
5	OMC-SO ₃ H ^b	1.3	42.1	61.5	58.3	34.6
6	OMC-SO ₃ H ^c	0.89	47.1	68.6	61.3	39.4
7	Amberlyst-15	4.7	58.9	83.8	75.2	50.3
8	SBA-15-SO ₃ H	1.26	40.5	69.2	61.5	30.9
9	GO	—	11.5	21.9	12.3	—
10	RGO	—	10.2	18.2	11.1	—

^a Measured by acid–base titration. ^b The reactions performed at static conditions. ^c Recycled 5 times.

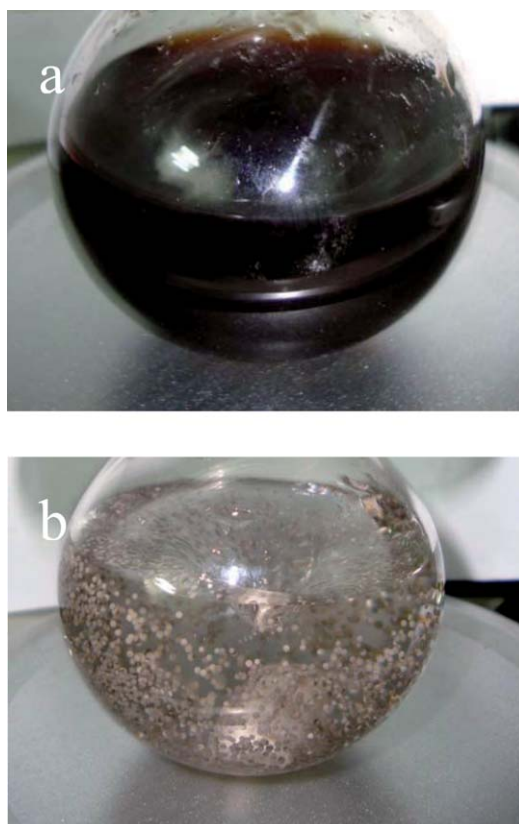


Fig. 9 Photographs of the esterification of acetic acid with cyclohexanol (EAC) over (a) G-SO₃H and (b) Amberlyst 15.

1–3 h, and the reaction rate gradually decreases; after 3 h, the reaction almost reaches equilibrium and the conversion is basically kept constant. For example, G-SO₃H gives conversions at

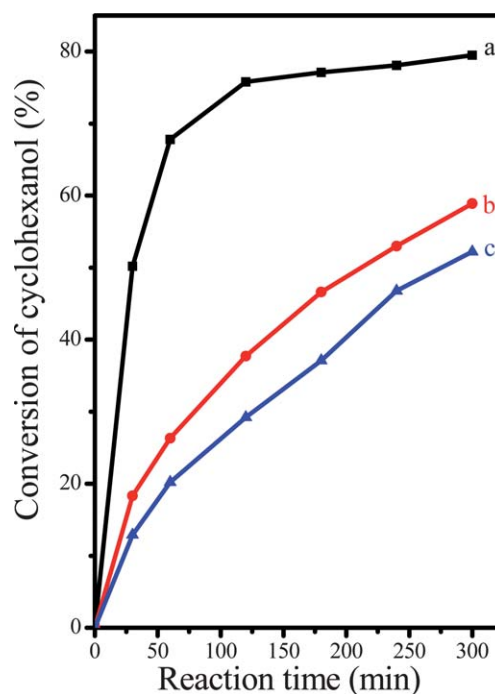


Fig. 10 Dependence of catalytic activities on the time for the esterification of acetic acid with cyclohexanol over (a) G-SO₃H, (b) Amberlyst 15, and (c) OMC-SO₃H.

1, 3, and 5 h of 67.9, 77.4, and 79.5%, respectively. In contrast, OMC-SO₃H and Amberlyst 15 have different kinetic curves. Even if the reaction time is 5 h, it still does not reach equilibrium for OMC-SO₃H and Amberlyst 15 catalysts.

Furthermore, the recyclability of G-SO₃H and OMC-SO₃H has been investigated. After being recycled 5 times, G-SO₃H still shows a high conversion (78.3%, Table 1, run 3), indicating that

there is almost no activity loss (0.8% loss for the activity). However, by the same number of recycles, OMC-SO₃H has a relatively high activity loss (9.7%, Table 1, run 6). The acid–base titration shows that recycling of the OMC-SO₃H catalyst leads to a partial loss of acidic sites (19.1% loss of total), while there is a relatively low loss of acidic sites (1.13 mmol g⁻¹, 5.8% loss) for G-SO₃H by the same treatment. The more stable sulfonic groups on G-SO₃H than OMC-SO₃H are closely related to the difference in the thermal stability of the sulfonic groups, as shown in Fig. 7. The stable sulfonic groups on G-SO₃H could be greatly important for practical applications of G-SO₃H as an efficient heterogeneous acidic catalyst in the future.

Moreover, the comparison of catalytic data over various catalysts is extended to EAB, PRE, and HPO. These reactions have similar catalytic trends to EAC. *i. e.* G-SO₃H exhibits much higher activities than OMC-SO₃H, Amberlyst 15, SBA-15-SO₃H, GO and RGO samples. For example, in EAB (Table 1, run 1, 4, 7–10), G-SO₃H shows an activity of 89.1%, while OMC-SO₃H, Amberlyst 15, SBA-15-Pr-SO₃H, GO and RGO have conversions of 75.1, 83.8, 69.2, 21.9 and 18.2%, respectively; in PRE (Table 1, run 1, 4, 7–10), G-SO₃H shows an activity of 82.1%, while OMC-SO₃H, Amberlyst 15, SBA-15-SO₃H, GO and RGO have conversions of 66.1, 75.2, 61.5, 12.3 and 11.1%, respectively; in HPO (Table 1, run 1, 4, 7, 8), G-SO₃H shows an activity of 66.8%, while OMC-SO₃H, Amberlyst 15, and SBA-15-Pr-SO₃H have conversions of 42.3, 50.3, and 30.9%, respectively. In addition, it is also worth noting that G-SO₃H has very good mass transfer in the reactions because the catalytic activities of the stirring conditions and static conditions are almost the same (Table 1, run 2 & 3), while there are obvious differences in the catalytic activities over OMC-SO₃H between the stirring and static conditions (Table 1, run 4 & 5), confirming that mass transfer influences catalytic activities in these reactions. For example, G-SO₃H exhibits a conversion of 89.3, 81.7, and 66.4% under static conditions in EAB, PRE, and HPO, which are very close to the activities (89.1, 82.1, and 66.8%) under stirring conditions. On the contrary, OMC-SO₃H shows that the activities (61.5, 58.3, and 34.6%) under static conditions are much lower than those (75.1, 66.1, and 42.3%) under stirring conditions. These results confirm that OMC-SO₃H has a limitation on mass transfer in these reactions. Furthermore, it is also observed that G-SO₃H has good recyclability in these reactions. For example, after being recycled 5 times, G-SO₃H shows conversions of 87.2, 80.8, and 64.9% in EAB, PRE, and HPO (Table 1, run 3). The activity loss in these reactions is only 1.5–2.8%. On the contrary, OMC-SO₃H has a significant reduction in the activities (6.9–9.8% loss, Table 1, run 6) after 5 recycles.

Conclusions

Sulfated graphene (G-SO₃H) is successfully synthesized from the hydrothermal sulfonation of reduced graphene oxide with fuming sulfuric acid at 180 °C. Catalytic tests in acid-catalyzed liquid reactions including the esterification of acetic acid with cyclohexanol, the esterification of acetic acid with 1-butanol, the Peckmann reaction of resorcinol with ethyl acetoacetate, and the hydration of propylene oxide show that G-SO₃H is a highly active, very stable, and excellently recyclable catalyst, which is strongly attributed to its unique graphene structure the fact that

there is almost no limitation of mass transfer for the catalytic reactions. This feature may be potentially important for industrial applications of G-SO₃H as an efficient catalyst in the future.

Acknowledgements

This work is supported by the State Basic Research Project of China (2009CB623507) and the National Natural Science Foundation of China (20973079 and U1162201).

Notes and references

- 1 A. Corma, *Chem. Rev.*, 1995, **95**, 559.
- 2 A. Corma, *Chem. Rev.*, 1997, **97**, 2373.
- 3 M. E. Davis, *Nature*, 2002, **417**, 813.
- 4 F. J. Liu, X. J. Meng, Y. L. Zhang, L. M. Ren, F. Nawaz and F.-S. Xiao, *J. Catal.*, 2010, **271**, 52.
- 5 C. W. Jones, K. Tsuji and M. E. Davis, *Nature*, 1998, **393**, 52.
- 6 D. Margolese, J. A. Melero, S. C. Christiansen, B. F. Chmelka and G. D. Stucky, *Chem. Mater.*, 2000, **12**, 2448.
- 7 J. A. Melero, R. Van Grieken and G. Morales, *Chem. Rev.*, 2006, **106**, 3790.
- 8 D. E. De Vos, M. Dams, B. F. Sels and P. A. Jacobs, *Chem. Rev.*, 2002, **102**, 3615.
- 9 P. Barbaro and F. Liguori, *Chem. Rev.*, 2009, **109**, 515.
- 10 M. Hara, T. Yoshida, A. Takagaki, T. Takata, J. N. Kondo, S. Hayashi and K. Domen, *Angew. Chem., Int. Ed.*, 2004, **43**, 2955.
- 11 M. Toda, A. Takagaki, M. Okamura, J. N. Kondo, S. Hayashi, K. Domen and M. Hara, *Nature*, 2005, **438**, 178.
- 12 T. A. Peters, N. E. Benes, A. Holmen and J. T. F. Keurentjes, *Appl. Catal. A*, 2006, **297**, 182.
- 13 J. J. Chiu, D. J. Pine, S. T. Bishop and B. F. Chmelka, *J. Catal.*, 2004, **221**, 400.
- 14 J. Perez-Ramirez, C. H. Christensen, K. Egeblad, C. H. Christensen and J. C. Groen, *Chem. Soc. Rev.*, 2008, **37**, 2530.
- 15 J. Karger and D. Freude, *Chem. Eng. Technol.*, 2002, **25**, 769.
- 16 B. J. Schoeman, J. Sterte and J. E. Otterstedt, *Zeolites*, 1994, **14**, 110.
- 17 L. Tosheva and V. P. Valtchev, *Chem. Mater.*, 2005, **17**, 2494–2513.
- 18 B. F. G. Johnson, *Top. Catal.*, 2003, **24**, 147.
- 19 C. J. H. Jacobsen, C. Madsen, J. Houzvicka, I. Schmidt and A. Carlsson, *J. Am. Chem. Soc.*, 2000, **122**, 7116.
- 20 Y. S. Tao, H. Kanoh, L. Abrams and K. Kaneko, *Chem. Rev.*, 2006, **106**, 896.
- 21 M. Choi, H. S. Cho, R. Srivastava, C. Venkatesan, D.-H. Choi and R. Ryoo, *Nat. Mater.*, 2006, **5**, 718.
- 22 W. Fan, M. A. Snyder, S. Kumar, P. S. Lee, W. C. Yoo, A. V. McCormick, R. L. Penn, A. Stein and M. Tsapatsis, *Nat. Mater.*, 2008, **7**, 984.
- 23 F.-S. Xiao, L. F. Wang, C. Y. Yin, K. F. Lin, Y. Di, J. Li, R. Xu, D. S. Su, R. Schlögl, T. Yokoi and T. Tatsumi, *Angew. Chem., Int. Ed.*, 2006, **45**, 3090.
- 24 M. Choi, K. Na, J. Kim, Y. Sakamoto, O. Terasaki and R. Ryoo, *Nature*, 2009, **461**, 246.
- 25 K. Na, C. Jo, J. Kim, K. Cho, J. Jung, Y. Seo, R. J. Messinger, B. F. Chmelka and R. Ryoo, *Science*, 2011, **333**, 328.
- 26 A. K. Geim, *Science*, 2009, **324**, 1530–1534.
- 27 K. S. Novoselov, A. K. Geim, S. V. Morozov, D. Jiang, Y. Zhang, S. V. Dubonos, I. V. Grigorieva and A. A. Firsov, *Science*, 2004, **306**, 666.
- 28 K. S. Novoselov, A. K. Geim, S. V. Morozov, D. Jiang, M. I. Katsnelson, I. V. Grigorieva, S. V. Dubonos and A. A. Firsov, *Nature*, 2005, **438**, 197.
- 29 S. Gilje, H. Song, M. Wang, K. L. Wang and R. B. Kaner, *Nano Lett.*, 2007, **7**, 3394.
- 30 H. B. Heersche, P. Jarillo-Herrero, J. B. Oostinga, L. M. K. Vandersypen and A. F. Morpurgo, *Nature*, 2007, **446**, 56.
- 31 D. H. Kim, J. H. Ahn, W. M. Choi, H. S. Kim, T. H. Kim, J. Z. Song, Y. G. Y. Huang, C. Liu and J. A. Rogers, *Science*, 2008, **320**, 507.
- 32 F. Schedin, A. K. Geim, S. V. Morozov, E. W. Hill, P. Blake, M. I. Katsnelson and K. S. Novoselov, *Nat. Mater.*, 2007, **6**, 652.
- 33 M. Zhou, Y. M. Zhai and S. J. Dong, *Anal. Chem.*, 2009, **81**, 5603.

- 34 Z. G. Xiong, L. L. Zhang and X. S. Zhao, *Chem.–Eur. J.*, 2011, **17**, 2428.
- 35 H. Zhang, X. J. Lv, Y. M. Li, Y. Wang and J. H. Li, *ACS Nano*, 2010, **4**, 380.
- 36 N. Severin, S. Kirstein, I. M. Sokolov and J. P. Rabe, *Nano Lett.*, 2009, **9**, 457.
- 37 Y. Ide, Y. Nakasato and M. Ogawa, *J. Am. Chem. Soc.*, 2010, **132**, 3601.
- 38 Y. G. Zhou, J. J. Chen, F. B. Wang, Z. H. Sheng and X. H. Xia, *Chem. Commun.*, 2010, **46**, 5951.
- 39 P. W. Sutter, J. I. Flege and E. A. Sutter, *Nat. Mater.*, 2008, **7**, 406.
- 40 Z. H. Tang, S. L. Shen, J. Zhuang and X. Wang, *Angew. Chem., Int. Ed.*, 2010, **49**, 4603.
- 41 G. M. Scheuermann, L. Rumi, P. Steurer, W. Bannwarth and R. Mülhaupt, *J. Am. Chem. Soc.*, 2009, **131**, 8262.
- 42 W. Chen, L. Duan, L. Wang and D. Zhu, *Environ. Sci. Technol.*, 2008, **42**, 6862.
- 43 G. Eda, G. Fanchini and M. Chhowalla, *Nat. Nanotechnol.*, 2008, **3**, 270.
- 44 X. Wang, L. J. Zhi and K. Mullen, *Nano Lett.*, 2008, **8**, 323.
- 45 E. Yoo, J. Kim, E. Hosono, H. Zhou, T. Kudo and I. Honma, *Nano Lett.*, 2008, **8**, 2277.
- 46 E. Beheshti, A. Nojeh and P. Servati, *Carbon*, 2011, **49**, 1561.
- 47 M. A. Worsley, P. J. Pauzauskie, T. Y. Olson, J. Biener, J. H. Satcher, Jr and T. F. Baumann, *J. Am. Chem. Soc.*, 2010, **132**, 14067.
- 48 A. K. Geim and K. S. Novoselov, *Nat. Mater.*, 2007, **6**, 183.
- 49 S. Stankovich, D. A. Dikin, G. H. B. Dommett, K. M. Kohlhaas, E. J. Zimney, E. A. Stach, R. D. Piner, S. T. Nguyen and R. S. Ruoff, *Nature*, 2006, **442**, 282.
- 50 J. S. Bunch, A. M. van der Zande, S. S. Verbridge, I. W. Frank, D. M. Tanenbaum, J. M. Parpia, H. G. Craighead and P. L. McEune, *Science*, 2007, **315**, 490.
- 51 W. S. Hummers, Jr and R. E. Offeman, *J. Am. Chem. Soc.*, 1958, **80**, 1339.
- 52 R. Xing, Y. M. Liu, Y. Wang, L. Chen, H. H. Wu, Y. W. Jiang, M. Y. He and P. Wu, *Microporous Mesoporous Mater.*, 2007, **105**, 41.
- 53 Y. C. Si and E. T. Samulski, *Nano Lett.*, 2008, **8**, 1679.
- 54 G. X. Zhao, L. Jiang, Y. D. He, J. X. Li, H. L. Dong, X. K. Wang and W. P. Hu, *Adv. Mater.*, 2011, **23**, 3959.
- 55 D. Long, W. Li, L. Ling, J. Miyawaki, I. Mochida and S.-H. Yoon, *Langmuir*, 2010, **26**, 16096.
- 56 X. Fan, W. Peng, Y. Li, X. Li, S. Wang, G. Zhang and F. Zhang, *Adv. Mater.*, 2008, **20**, 4490.
- 57 F. Tuinstra and J. L. Koenig, *J. Chem. Phys.*, 1970, **53**, 1126.
- 58 Z. Lin, Y. Yao, Z. Li, Y. Liu, Z. Li and C.-P. Wong, *J. Phys. Chem. C*, 2010, **114**, 14819.
- 59 G. Eda and M. Chhowalla, *Adv. Mater.*, 2010, **22**, 2392.
- 60 E. B. Orler, D. J. Yontz and R. B. Moore, *Macromolecules*, 1993, **26**, 5157.
- 61 S. Suganuma, K. Nakajima, M. Kitano, H. Kato, A. Tamura, H. Kondo, Yanagawa, S. Hayashi and M. Hara, *Microporous Mesoporous Mater.*, 2011, **443**, 143.
- 62 A. K. Geim and K. S. Novoselov, *Nat. Mater.*, 2007, **6**, 183.